Journal of Alloys and Compounds 867 (2021) 159059

Contents lists available at ScienceDirect

Journal of Alloys and Compounds

journal homepage: www.elsevier.com/locate/jalcom

Crystal structure, Raman spectra and microwave dielectric properties of novel low-temperature cofired ceramic Li_4GeO_4

Zijian Yang[a,b], Ying Tang[a,b,*], Jie Li[a,b,*], Weishuang Fang[a,b], Jinyan Ma[a,b], Aihong Yang[a,b], Laijun Liu[a,b], Liang Fang[a,b,*]

[a] Guangxi Key Laboratory of Optical and Electronic Materials and Devices, College of Material Science and Engineering, Guilin University of Technology, Guilin 541004, China
[b] Key Laboratory of Nonferrous Materials and New Processing Technology, Ministry of Education, Guilin University of Technology, Guilin 541004, China

ARTICLE INFO

Article history:
Received 1 August 2020
Received in revised form 25 January 2021
Accepted 2 February 2021
Available online 6 February 2021

Keywords:
Li_4GeO_4
Olivine structure
LTCC
Microwave dielectric property

ABSTRACT

A low-permittivity and low-loss ceramic, Li_4GeO_4, was fabricated via solid state reaction route. XRD showed that a single orthorhombic Li_4GeO_4 phase with olivine structure was prepared over the sintering temperature range of 660–740 °C. Dense ceramic sintered at 720 °C revealed excellent microwave properties, with ε_r ~6.99, $Q \times f$ ~47,813 GHz (at 15.5 GHz), and τ_f ~ − 159.2 ppm/°C. The microwave dielectric performances were analyzed with the intrinsic characteristics of crystal structure by ionic polarizability and Raman spectra. Additionally, the Li_4GeO_4 ceramic showed good chemical compatibility with Ag sintered at 720 °C. In the low-temperature cofired ceramic (LTCC) application, aforesaid results manifested that Li_4GeO_4 ceramic was considered as a potential candidate.

1. Introduction

In the last decades, microwave dielectric materials have experienced enormous progress with a wide range of applications in filters, resonators, substrates, and antennas, etc. The recent advances in wireless communication and information systems have stimulated the development of new materials and technologies [1,2]. One of the development directions is the high-frequency dielectric materials for the next generation communication system. The signal transmission speed is proportional to the square root of dielectric constant (ε_r). Hence, the low permittivity is profitable to increase the signal propagation velocity. Meanwhile, for better frequency selectivity, high filter performances, and reduced insertion loss, low dielectric losses (tanδ) or high Q values (Q = 1/tanδ) are crucial for the development of novel materials that can be used at high-frequency bands [3,4]. Hence, seeking for such ceramic materials with low permittivity and the optimization of process becomes a urgent demand in the development of wireless communications. In terms of the optimization of process, the low temperature co-fired ceramic (LTCC) technology is being increasingly crucial, which can integrate a combination of multichip modules to satisfy the increasing needs for integration and miniaturization [5,6]. Additionally, the dielectric ceramics should possess good chemical compatibility with inner metal electrodes.

In the past several years, some germanate ceramics such as Zn_2GeO_4 [7], Mg_2GeO_4 [8], Ca_2GeO_4 [9], $CaMgGeO_4$ [10], $MgGeO_3$ [11] have been reported as potential dielectric materials with low-ε_r. These ceramics exhibited a low ε_r in the range of 6.7 ~ 7.1, a high $Q \times f$ value varying from 95,000 to 124,000 GHz and a relatively large negative τ_f between − 27 and − 75 ppm/°C. However, the high sintering temperature above 1100 °C limited its practical applications in LTCC [12–15]. A variety of Li-containing germanates with low ε_r and their sintering temperatures were reported. For instance, the excellent dielectric properties of $Li_2ZnGe_3O_8$, that is, ε_r ~ 10.3, $Q \times f$ ~47,400 GHz and τ_f ~− 63.9 ppm/°C were reported by Xiang et al. [17] Olivine-structure ceramics were also characterized with low ε_r and high $Q \times f$ value, like Li_2MGeO_4 (M = Mg and Zn) with ε_r = 6.1 ~ 6.5, $Q \times f$ = 28,500–35,400 GHz and τ_f = −74.7–− 60.6 ppm/°C [18].

With view to further reduce the sintering temperature, 2 Li^+ ions might be introduced to substitute 1 M cation in Li_2MGeO_4 (M=Zn, Mg) to synthesize Li_4GeO_4 ceramics. Li_4GeO_4 was firstly reported to have olivine structure by Voellenkle et al.[19], then the low conductivity at room temperature (3.1×10^{-12} Om^{-1} cm^{-1}) [20] vibrational spectra and energy characteristics of Li_4GeO_4 were

* Corresponding authors at: Guangxi Key Laboratory of Optical and Electronic Materials and Devices, College of Material Science and Engineering, Guilin University of Technology, Guilin 541004, China
E-mail addresses: tangyinggl001@aliyun.com (Y. Tang), jielee@glut.edu.cn (J. Li), fanglianggl001@aliyun.com (L. Fang).

https://doi.org/10.1016/j.jallcom.2021.159059
0925-8388/

studied [21]. However, few studies have been conducted about the microwave dielectric properties of Li_4GeO_4. In consideration of Li_4GeO_4 having the advantage of low conductivity, low permittivity and low synthesis temperature, novel microwave dielectric ceramics Li_4GeO_4 were synthesized. The phase evolution, sintering behaviors and the relationship between dielectric properties and Raman modes of Li_4GeO_4 ceramics were studied detailly.

2. Experimental procedure

Raw materials, high purity Li_2CO_3 and GeO_2 (≥ 99.99%), were prepared as the pure Li_4GeO_4 ceramics via standard solid-state sintering technique. The stoichiometric raw powders were mixed with ethanol and zirconia balls as medium for 6 h, the slurries were dried and then calcined at 600 °C for 6 h. The calcined powders were ball-milled and dried again under the same conditions, and then pressed into cylinders of 10 mm × 6.5 mm size using 5 wt% PVA as a binder. The pellets were sintered at 660–740 °C for 6 h with a heating rate of 5 °C·min^{-1}.

The apparent density was obtained by Archimedes method. The X-ray diffraction (XRD, X'pert PRO, Holland) was employed to evaluate the phase purity and structure. Rietveld refinement was operated to study the crystal structure of Li_4GeO_4 ceramics by the FullProf software. The Raman spectra of Li_4GeO_4 ceramics were performed on Raman spectrometer (DXR, Thermo Fisher Scientific, USA). The superficial microstructure of samples was observed by field-emission scanning electron microscopy (SEM, Hitachi S4800, Japan). The dielectric properties (ε_r, $Q \times f$, τ_f) of Li_4GeO_4 ceramics were measured by a vector network analyzer (Model N3230A, Agilent, USA) with the Hakki and Coleman resonator method. The τ_f values were attained from the change of the resonant frequency between 25 ℃ and 85 ℃ with a temperature chamber. Thermal dilatometer (DIL402PC, NETZSCH, Germany) was handled to complete the linear coefficient of thermal expansion (CTE).

3. Result and discussion

The X-ray diffraction of Li_4GeO_4 ceramics sintered at 660–740 °C, are presented in Fig. 1, clarifying the sintering dependence of crystalline phase of Li_4GeO_4. Based on JCPDS 01-072-1587 for Li_4GeO_4, all the diffraction peaks indexed well with the standard card of olivine Li_4GeO_4 phase, with orthorhombic structure in space group B*mmb*,

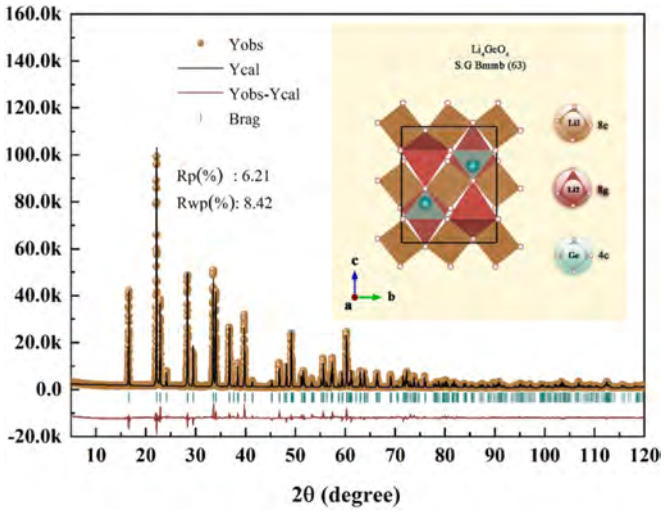

Fig. 2. The Rietveld refinement on the X-ray powder diffraction patterns of Li_4GeO_4 sintered at 720 °C/4 h and the structure diagram of Li_4GeO_4.

without any other phases. The result indicated that Li_4GeO_4 ceramics belonged to a single phase and kept stable between 660 °C and 740 °C. The enlarged area in Fig. 1 exhibits the variation in main peak (111) of Li_4GeO_4 ceramic with increasing sintering temperature. Obviously, the diffraction peak (111) firstly moves towards the lower angle to the minimum value (at 720 °C), then shifts towards the higher angle at 740 °C, indicating the first increase and decrease in cell volume.

The refined profile of Li_4GeO_4 ceramics sintered at 720 °C by the Rietveld method is given in Fig. 2. The experimental data fitted the refined patterns, and the reliability factors were acceptable with the profile of R_p = 6.21% and R_{wp} = 8.42%. Based on the refinement result, the cell parameters were a = 7.7725(0) Å, b = 6.0553 (1) Å, c = 7.3653(1) Å and V = 346.6465(1) Å^3. Meanwhile, the schematic of the crystal structure of Li_4GeO_4 ceramics is exhibited in the inset of Fig. 2, olivine structural Li_4GeO_4 has a cationic distribution of $[Li1]^2[Li2]^2GeO_4$, which is composed of three different tetrahedrons $[Li1O_4]$, $[Li2O_4]$ and $[GeO_4]$. In the structure, chains are composed of $[GeO_4]$ and $[LiO_4]$ tetrahedrons with two different positions, each

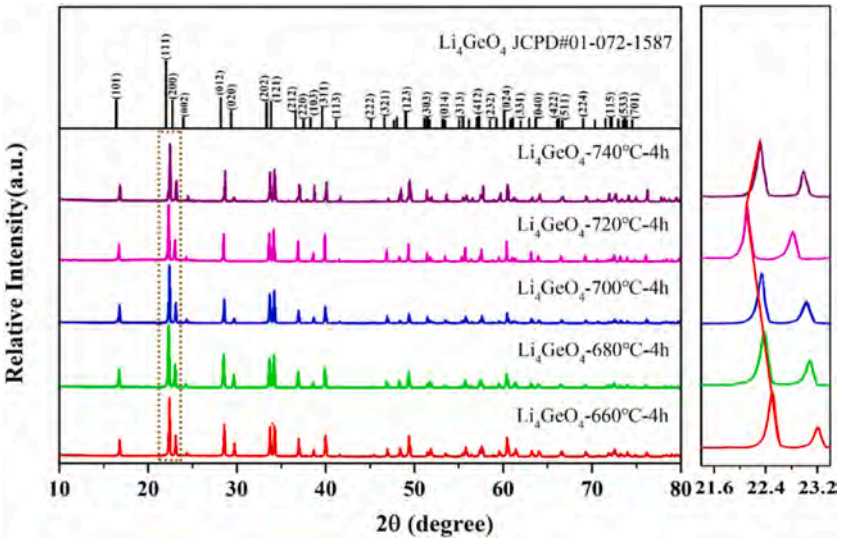

Fig. 1. The XRD patterns of the Li_4GeO_4 ceramics sintered at different temperatures for 4 h.

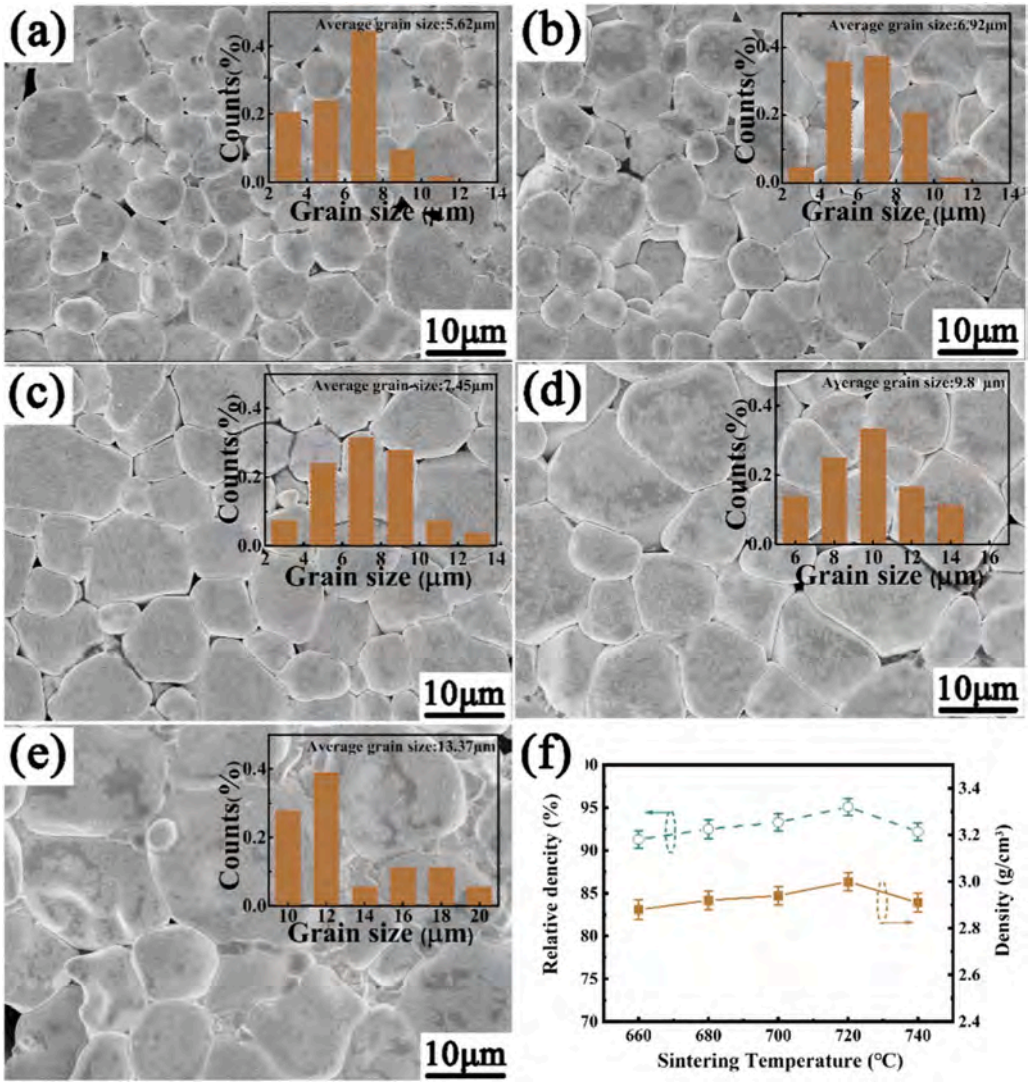

Fig. 3. (a)–(e) SEM images of thermal etched surfaces (the grain size distribution histogram inserted), (f) bulk and relative densities of Li_4GeO_4 ceramics sintered from 660° to 740 °C.

distorted [GeO_4] tetrahedrons is corner-sharing with [$Li2O_4$] and [$Li1O_4$] tetrahedrons, forming a three-dimensional framework.

SEM images of the thermal etched surfaces were recorded to examine the surface morphology of Li_4GeO_4 samples sintered at 660–740 °C (Fig. 3(a–e)). The grain sizes showed slightly increasing trend as sintering temperature increased. When sintering temperature reaching 720 °C, the Li_4GeO_4 ceramic gained the maximum grain size of 8–12 μm and dense microstructure, whereas grains began to grow abnormally with slight porosity when sintered at 740 °C. Fig. 3(f) illustrated the variation tendency of the bulk density and relative density with sintering temperature. The bulk densities firstly gradually increased from 2.08 g/cm^3 (91.3% relative density) at 660 °C to the optimal value of 3.01 g/cm^3 (95.1% relative density) at 720 °C. Nevertheless, the bulk densities decreased slightly when the temperature exceeding 720 °C, which could attribute to this fact that abnormal growth of grains caused by high temperature destroyed the uniformity of grains.

The variation of microwave dielectric properties of Li_4GeO_4 ceramics in connection with sintering temperature are plotted in Fig. 4. The permittivity fluctuated around 6.89 within the sintering temperature scope of 660–740 °C (Fig. 4(a)). As we all know, there are many elements that influence the dielectric constant (ε_r) at microwave frequencies, for example, the density, the second phases and the ionic polarizability, etc. Here, the theoretical permittivity (ε_{th}) of Li_4GeO_4 was available by Clausius-Mossotti equation [23]:

$$\varepsilon_{th} = \frac{3V + 8\pi a}{3V - 4\pi a} \quad (1)$$

In which, α and V referred to the molecular polarizability and the cell volume, respectively. The ε_{th} of Li_4GeO_4 was 7.98. Besides, the ε_r could be amended by Bosman and Having's formula to eliminate the effect of porosity:

$$\varepsilon_{corr} = \varepsilon_r \quad (1 + 1.5 \quad p) \quad (2)$$

in which, p was the fractional porosity. The ε_{corr} value of Li_4GeO_4 sintered at 720 °C was 7.76. The relative error between ε_{corr} and ε_{th} was 2.75%, indicating ionic polarization being the main factor in the dielectric polarizability in microwave frequency band [24].

As observed from Fig. 4(b), the $Q \times f$ values of Li_4GeO_4 ceramics exhibited similar variation trend to the relative densities, and optimal $Q \times f$ value of 47,813 GHz (f = 15.5 GHz) for Li_4GeO_4 ceramics were acquired at 720 °C. As known, the dielectric loss at microwave

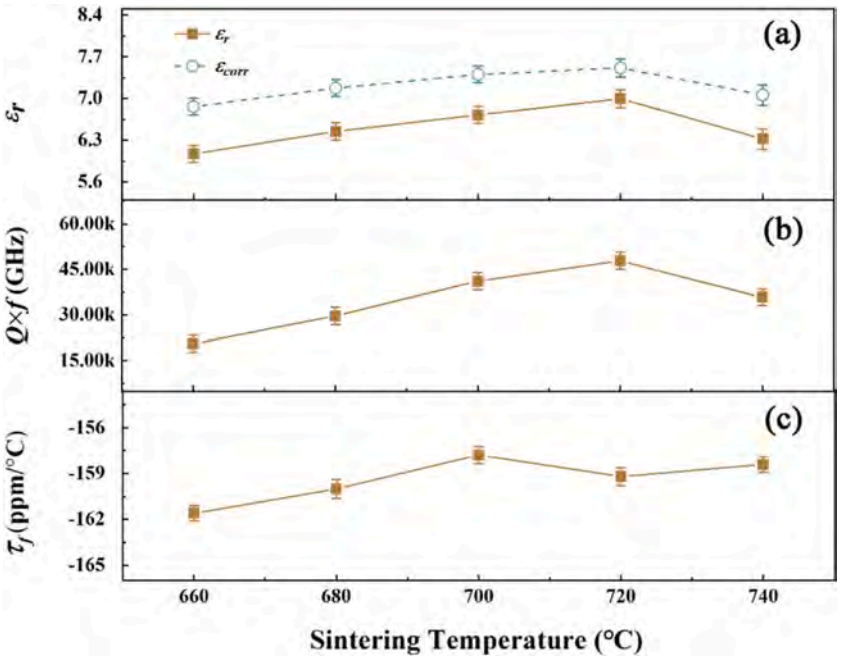

Fig. 4. Microwave dielectric properties of Li_4GeO_4 ceramics as a function of sintering temperature from 660° to 740 °C: (a) ε_r, (b) $Q\times f$ and (c) τ_f.

frequency region is influenced by two categories: the internal factors largely relied on inharmonic vibrations and the external ones, such as grain size, point defects and impurities [25]. The τ_f value remained around − 160 ppm/°C and was less reliant on sintering temperature (Fig. 4(c)). For low-permittivity microwave dielectric ceramics, ionic displacement polarizations play a dominant role in controlling the ε_r value. Therefore, the τ_f value can be determined as follows:

$$\tau_f = -\left(\frac{\tau_\varepsilon}{2} + \alpha_L\right) \quad (3)$$

in which, τ_ε and α_L is the temperature coefficient of permittivity and the linear thermal expansion coefficient, respectively. According to the thermal expansion data (Fig. 5), the α_L of Li_4GeO_4 ceramic is 3.9 ppm/°C between 25 °C and 85 °C. And, the τ_ε value has been measured as 288.42 ppm/°C at the microwave band using the Hakki-Coleman method between 25 °C and 85 °C. Hence, the τ_f value for Li_4GeO_4 ceramic can been calculated from the Eq. (3) as − 148.11 ppm/°C, which is close to the measured τ_f value (−159.2 ppm/°C) using the Hakki-Coleman method in the same temperature range.

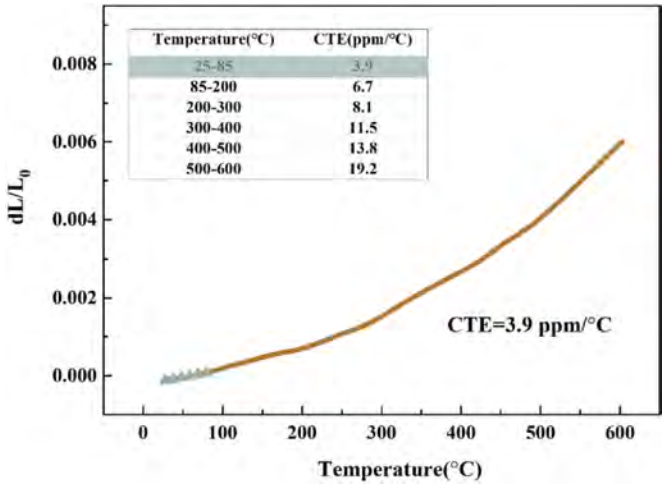

Fig. 5. Thermal expansion curve in the temperature range of 25–600 °C of Li_4GeO_4 sintered at 720 °C.

Raman spectroscopy was performed to provide local structure information and study the related vibrational characteristic to microwave dielectric properties. Fig. 6 shows the Raman spectra of the Li_4GeO_4 ceramics sintered at various temperatures in the range of

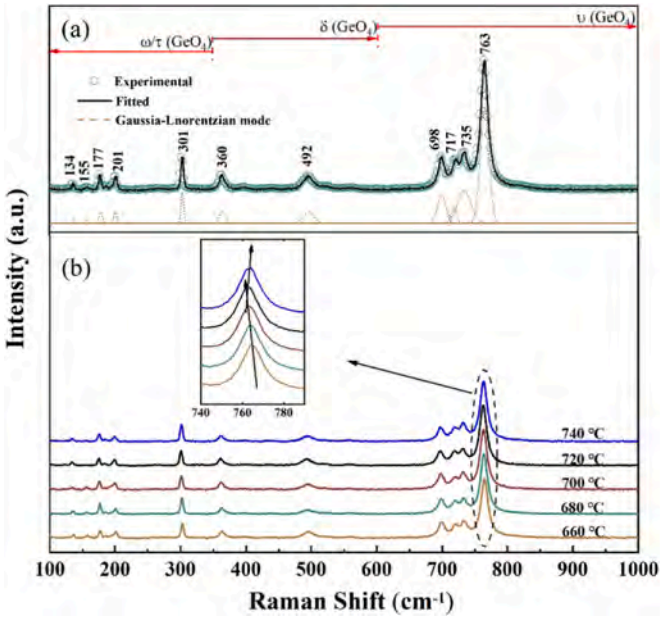

Fig. 6. (a) Fitting results of the Li_4GeO_4 sample sintered at 720 °C as a representative; (b) Room-temperature Raman spectra for the Li_4GeO_4 samples sintered at various temperatures in the range of 100–1000 cm^{-1}.

Table 1
The Raman active modes of experiment for Li_4GeO_4 ceramic sintered at 720 °C and compared with data of literatures.

Band	Roman active modes (cm^{-1})		Symmetry modes	Assignments
	Observation	Literature		
1	134	110	B_1g	T Ge/Ge
2	155	184	B3g	T Li/Li
3	177	202	B2g	T Ge/Ge
4	201	216	Ag	T Li/Li
5	301	282	Ag	R + T Li/Li
6	360	361	B2g	R + T Li/Li
7	492	497	Ag	δ O-Ge-O
8	698	673	Ag	ν3 GeO4
9	717	688	B3g	ν3 GeO4
10	735	717	B1g	ν3 GeO4
11	763	737	A_g	ν_1 GeO_4

100–1000 cm^{-1}. Based on the group theory, the Raman active modes of space group *Bmmb* can be summarized as [21]:

$$\Gamma_{Raman} = 8A_g + 7B_{1g} + 6B_{2g} + 6B_{3g} \quad (4)$$

Not all vibrational modes could be observed on account of the overlap of the Raman active modes and the assignments of Li_4GeO_4

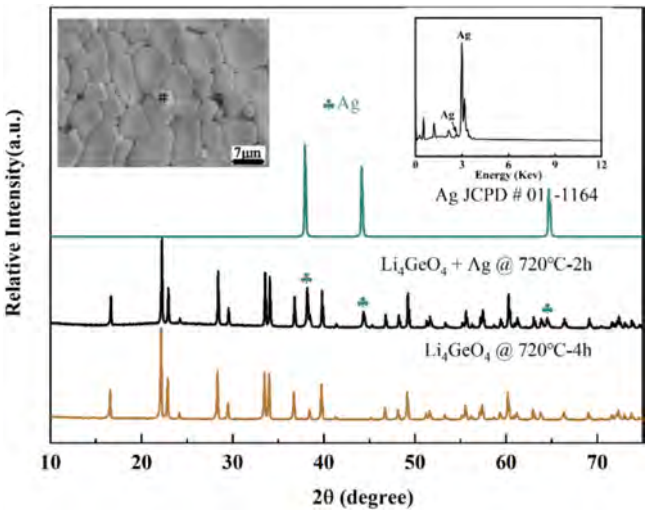

Fig. 8. The XRD patterns of Li_4GeO_4 + Ag samples sintered at 720 °C for 2 h; BSEM analysis of Li_4GeO_4 ceramic cofired with 20 wt% Ag at 720 °C for 2 h.

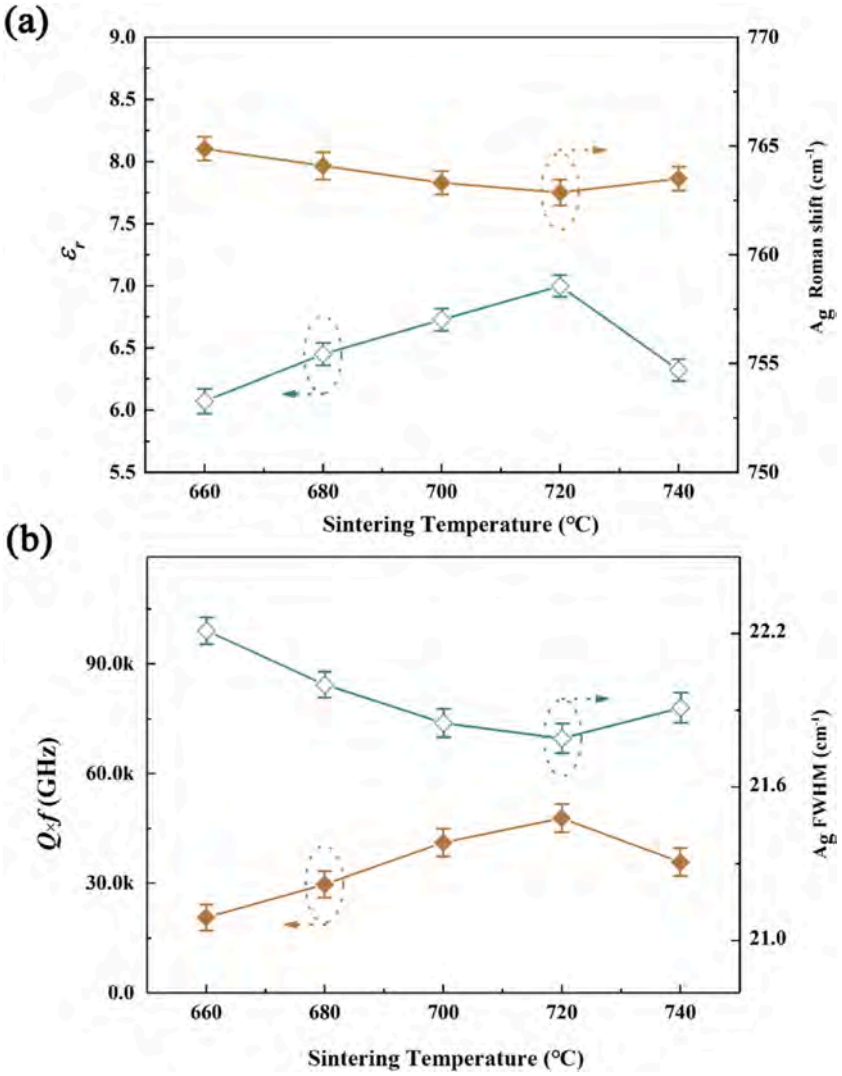

Fig. 7. The relationship between A_{1g} mode and microwave dielectric properties (ε_r, $Q \times f$ and τ_f values) of Li_4GeO_4 ceramics as a function of sintering temperature.

ceramic sintered at 720 °C are listed in Table 1. According to the previous report of Fomichev [21,26], the weaken peaks, locked at 134, 155, 177 and 201 cm^{-1} were mainly attributed to the translation of Li^+ and Ge^{4+} ions. For the mode 5 at 301 cm^{-1}, the rotation and translation of Li^+ were widely perceived as the contributing to Raman peak. The frequencies at the range of 360–600 cm^{-1} were assigned to O-Ge-O bending mode (360 cm^{-1}) and Li^+ translation and rotational mode (301 cm^{-1}). The peaks locked at 600–1000 cm^{-1} were related to the internal stretching vibrations of the [GeO_4] tetrahedra. Additionally, the enlarged area of Fig. 6(b) exhibits the variational Roman shift in the region of 740–790 cm^{-1}. As the temperature rose, the peak 11 moved toward low frequency and then shifted to high frequency. A slight expansion in the [GeO_4] tetrahedra might account for the red shift, while the blue shift could be analyzed by the shrinking in the [GeO_4] tetrahedra.

The Raman shifts, the Raman fullwidth at half maximum (FWHM) of vibration mode at 763 cm^{-1} assigned to the A_g mode, and microwave dielectric properties of Li_4GeO_4 are plotted in Fig. 7. Quiet sensitive to the crystal structure, Raman spectroscopy is considered as an effective measure to explore the relevance between microwave dielectric properties and lattice vibrations [26]. In the case, the peak 11 was caused by the internal stretching vibration of [GeO_4] tetrahedra. The red shift of mode 11 revealed the increase in volume of oxygen tetrahedra, and that would exert influence on the polarization of Ge^{4+} in the [GeO_4] tetrahedra. As shown in Fig. 7(a), the variation of Raman shift with sintering temperature was opposite to the change of ε_r, which was owing to substantial Raman shift corresponding to high vibration energy of oxygen tetrahedra, rigid oxygen tetrahedra providing small space for cation vibrations, resulting in a lower ε_r [27,28]. Similarly, the FWHM was lowered and then heightened as temperature increased, which was contrary to the variation of $Q \times f$ (Fig. 7(b)). This attributed to the weakening of the damping behavior of 763 cm^{-1} mode as its FWHM lowered, in turn to decrease the intrinsic dielectric loss [26].

The Li_4GeO_4 ceramic powders were chosen to co-fired with 20 wt% silver powders at 720 °C/2 h, to analyze the chemical compatibility with the silver electrode Fig. 8 displays the XRD, BSEM and EDS results of the co-fired ceramics. There was no other phase found except for the orthorhombic Li_4GeO_4 and Ag, which meant that Li_4GeO_4 did not react with silver. Two different shaped grains with distinct sizes were clearly distinguished from the BSE image, and the larger grains were Ag from EDS results. Therefore, it could be confirmed that Li_4GeO_4 ceramic was chemically compatible with silver electrodes.

4. Conclusion

The Li_4GeO_4 ceramics with low ε_r were synthesized by solid state reaction. Rietveld refinement of XRD proved that Li_4GeO_4 phase belonged to orthorhombic structure with space group B*mmb*. The optimal microwave dielectric properties with $\varepsilon_r \sim 6.99$, $\tau_f \sim -159.2$ ppm/°C, $Q \times f \sim 47{,}813$ GHz (at 15.5 GHz) were measured in the Li_4GeO_4 ceramic sintered at 720 °C. The variation in the ε_r and $Q \times f$ values were inversely correlated to the Roman shift and FWMH, respectively. The low intrinsic sintering temperature, low ε_r, excellent microwave dielectric properties and good chemical compatibility with Ag suggest that Li_4GeO_4 ceramic is a promising alternative for LTCC applications.

CRediT authorship contribution statement

Zijian Yang: Data Curation, Writing - original draft preparation. **Ying Tang:** Funding acquisition. **Jie Li:** Supervision , Formal analysis, Writing - review & editing. **Weishuang Fang:** Data curation. **Jinyan Ma:** Data curation. **Aihong Yang:** Data curation. **Laijun Liu:** Data curation. **Liang Fang:** Resources, Supervision, Funding acquisition.

Declaration of Competing Interest

The authors declare that they have no known competing financial interests or personal relationships that could have appeared to influence the work reported in this paper.

Acknowledgments

This work was supported by the Natural Science Foundation of China (Nos. 21761008 and 21965009), the Natural Science Foundation of Guangxi Zhuang Autonomous Region (Nos. 2018GXNSFAA138175), and the Supported of Open Foundation of Guangxi Key Laboratory of Optical and Electronic Materials and Devices (20AA-16 and 20AA-11) and Foundation of Guilin University of Technology (GUTQDJJ2019183), the Project funded by China Postdoctoral Science Foundation (2020M683628XB) and High level innovation team and outstanding scholar program of Guangxi Institutes and Innovation Project of Guangxi Graduate Education (YCBZ2020167 and YCBZ2020066).

References

[1] Z.Y. Zou, Z.H. Chen, X.K. Lan, W.Z. Lu, B. Lua, B. Ullah, X.H. Wang, W. Lei, Weak ferroelectricity and low-permittivity microwave dielectric properties of $Ba_2Zn_{(1+x)}Si_2O_{(7+x)}$ ceramics, J. Eur. Ceram. Soc. 37 (2017) 3065–3071.
[2] H.Z. Zuo, X.L. Tang, H.W. Zhang, Y.M. Lai, Y.L. Jing, H. Su, Low-dielectric-constant $LiAlO_2$ ceramics combined with LBSCA glass for LTCC applications, Ceram. Int. 43 (2017) 8951–8955.
[3] B. Tang, S.Q. Yu, H.T. Chen, S.R. Zhang, X.H. Zhou, Phase structure and microwave dielectric properties of $Zr(Zn_{1/3}Nb_{2/3})_xTi_{2-x}O_6$ ($0.2 \le x \le 0.8$) ceramics, J. Mater. Sci. Mater. Electron. 24 (2013) 1475–1479.
[4] T. Teranishi, R. Kanemoto, H. Hayashi, A. Kishimoto, Effect of the (Ba+Sr)/Ti ratio on the microwave-tunable properties of $Ba_{0.6}Sr_{0.4}TiO_3$ ceramics, J. Am. Ceram. Soc. 100 (2017) 1037–1043.
[5] H. Jantunen, R. Rautioaho, A. Uusimäki, S. Leppavuori, Compositions of $MgTiO_3$–$CaTiO_3$ ceramic with two borosilicate glasses for LTCC technology, J. Eur. Ceram. Soc. 20 (2000) 2331–2336.
[6] W. Lei, W.Z. Lu, X.C. Wang, Temperature compensating $ZnAl_2O_4$–Co_2TiO_4 spinel-based low-permittivity microwave dielectric ceramics, Ceram. Inter 38 (2012) 99–103.
[7] S. Wu, Q. Ma, Synthesis, characterization and microwave dielectric properties of Zn_2GeO_4 ceramics, J. Alloy. Compd. 567 (2013) 40–46.
[8] C.X. Chen, S.P. Wu, J.H. Li, Synthesis and microwave dielectric properties of B_2O_3-doped Mg_2GeO_4 ceramics, J. Alloy. Compd. 578 (2013) 153–156.
[9] Y. Tang, M.Y. Xu, L. Duan, J.Q. Chen, C.C. Li, H.C. Xiang, L. Fang, Structure, microwave dielectric properties, and infrared reflectivity spectrum of olivine type Ca_2GeO_4 ceramic, J. Eur. Ceram. Soc. 39 (2019) 2354–2359.
[10] H.C. Xiang, C.C. Li, H. Jantunen, L. Fang, A. Hill, An ultra-low loss $CaMgGeO_4$ microwave dielectric ceramic and its chemical compatibility with silver electrodes for LTCC applications, ACS Sustain. Chem. Eng. 6 (2018) 6458–6466.
[11] W.S. Fang, K. Cheng, H.C. Xiang, Y. Tang, Y.F. Zhai, C.X. Su, L. Fang, Phase composition and microwave dielectric properties of low permittivity $AGeO_3$ (A = Mg, Zn) ceramics, J. Alloy. Compd. 799 (2019) 495–500.
[12] D. Zhou, J. Li, L.X. Pang, D.W. Wang, I.M. Reaney, Novel water insoluble $(Na_xAg_{2x})MoO_4$ ($0 \le x \le 2$) microwave dielectric ceramics with spinel structure sintered at 410 degrees, J. Mater. Chem. C 24 (2017) 6086–6091.
[13] D. Zhou, L.X. Pang, D.W. Wang, H.H. Guo, F. Yang, Z.M. Qi, C. Li, B.B. Jin, I.M. Reaney, Crystal structure, impedance and broadband dielectric spectra of ordered scheelite-structured $Bi(Sc_{1/3}Mo_{2/3})O_4$ ceramic, J. Eur. Ceram. Soc. 38 (2018) 1556–1561.
[14] S.Z. Hao, D. Zhou, F. Hussain, W.F. Liu, J.Z. Su, D.W. Wang, Q.P. Wang, Z.M. Qi, C. Singh, S. Trukhanov, Structure, spectral analysis and microwave dielectric properties of novel $x(NaBi)_{0.5}MoO_4$-$(1-x)Bi_{2/3}MoO_4$ (x = 0.2 ~ 0.8) ceramics with low sintering temperatures, J. Eur. Ceram. Soc. 40 (2020) 3569–3576.
[15] D. Zhou, L.X. Pang, D.W. Wang, Z.M. Qi, I.M. Reaney, High quality factor, ultralow sintering temperature $Li_6B_4O_9$ microwave dielectric ceramics with ultralow density for antenna substrates, ACS Sustain. Chem. Eng. 6 (2018) 11138–11143.
[17] H.C. Xiang, L. Fang, W.S. Fang, Y. Tang, C.C. Li, A novel low-firing microwave dielectric ceramic $Li_2ZnGe_3O_8$ with cubic spinel structure, J. Eur. Ceram. Soc. 37 (2017) 625–629.
[18] C.C. Li, H.C. Xiang, M.Y. Xu, Y. Tang, L. Fang, Li_2AGeO_4 (A= Zn, Mg): two novel low-permittivity microwave dielectric ceramics with olivine structure, J. Eur. Ceram. Soc. 38 (2017) 1524–1528.
[19] H. Voellenkle, A. Wittmann, Z. Kristallogr, Die kristallstruktur von Li_4GeO_4, Zeitschrift für Kristallographie-Crystalline, Materials 128 (1969) 66–71.
[20] I.M. Hodge, M.D. Ingram, A.R. West, Ionic conductivity of Li_4SiO_4, Li_4GeO_4, and their solid solutions, J. Am. Ceram. Soc. 59 (1976) 360–366.

[21] V.V. Fomichev, E.V. Proskuryakova, Vibrational spectra and energy characteristics of the superionics Li_4SiO_4 and Li_4GeO_4, J. Solid State Chem. 134 (1997) 232–237.
[23] R.D. Shannon, Dielectric polarizabilities of ions in oxides and fluorides, J. Appl. Phys. 73 (1993) 348–366.
[24] S.H. Yoon, D.W. Kim, S.Y. Cho, K.S. Hong, Investigation of the relations between structure and microwave dielectric properties of divalent metal tungstate compounds, J. Eur. Ceram. Soc. 26 (2006) 2051–2054.
[25] S.H. Yoon, G.K. Choi, D.W. Kim, S.Y. Cho, K.S. Hong, Mixture behavior and microwave dielectric properties of (1-x)$CaWO_4$-xTiO_2, J. Eur. Ceram. Soc. 27 (2007) 3087–3091.
[26] S.M. Wan, S.J. Zhang, X.Y. Going, Y. Zeng, S.J. Jiang, J.L. You, Structural investigations on two typical lithium germanate melts by in situ Raman spectroscopy and density functional theory calculations, Cryst. Eng. Comm. 22 (2020) 701–707.
[27] S.K. Singh, V.R.K. Murthy, Microwave dielectric properties of $Li_2SrTa_{2(1-x)}Nb_{2x}O_7$ ceramics investigated by Raman spectroscopy, Ceram. Inter. 42 (2016) 7284–7289.
[28] Y. Wu, D. Zhou, J. Guo, L.X. Pang, H. Wang, X. Yao, Temperature stable microwave dielectric ceramic $0.3Li_2TiO_3$-$0.7Li(Zn_{0.5}Ti_{1.5})O_4$ with ultra-low dielectric loss, Mater. Lett. 65 (2011) 2680–2682.